# 2011 LLNL Nuclear Forensics Summer Program

Glenn T. Seaborg Institute
Lawrence Livermore National Laboratory
Physical and Life Sciences
Livermore, CA 94550, USA

Director: Annie Kersting (kersting1@llnl.gov)
Education Coordinator: Nancy Hutcheon
Administrator: Camille Vandermeer
Website https://seaborg.llnl.gov

**Sponsors:**
National Technical Nuclear Forensics Center, Domestic Nuclear Detection Office, Department of Homeland Security
LLNL: Glenn T. Seaborg Institute, Physical and Life Sciences Directorate

LLNL-TR-502460

The Lawrence Livermore National Laboratory (LLNL) Nuclear Forensics Summer Program is designed to give both undergraduate and graduate students an opportunity to come to LLNL for 8-10 weeks during the summer for a hands-on research experience. Students conduct research under the supervision of a staff scientist, attend a weekly lecture series, interact with other students, and present their work in poster format at the end of the program. Students also have the opportunity to participate in LLNL facility tours (e.g. National Ignition Facility, Center of Accelerator Mass-spectrometry) to gain a better understanding of the multi-disciplinary science that is on-going at LLNL.

Currently called the Nuclear Forensics Summer Program, this program began 11 years ago as the Actinide Sciences Summer Program. The program is run within the Glenn T. Seaborg Institute in the Physical and Life Sciences Directorate at LLNL. The goal of Nuclear Forensics Summer Program is to facilitate the training of the next generation of nuclear scientists and engineers to solve critical national security problems in the field of nuclear forensics. We select students who are majoring in physics, chemistry, nuclear engineering, chemical engineering and environmental sciences. Students engage in research projects in the disciplines of actinide and radiochemistry, isotopic analysis, radiation detection, and nuclear engineering in order to strengthen the 'pipeline' for future scientific disciplines critical to DHS (DNDO), NNSA.

This is a competitive program with over 150 applicants for the 8-10 slots available. Students come highly recommended from universities all over the country. For example, this year we hosted students from Clemson University, South Carolina, University of North Carolina, University of Minnesota, University of Notre Dame, and University of California, at Berkeley and at Santa Barbara (See Table 1). We advertise with mailers and email to physics, engineering, geochemistry and chemistry departments throughout the U.S. We also host students for a day at LLNL who are participating in the D.O.E. sponsored "*Summer School in Radiochemistry"* course held at San Jose State University and have recruited from this program. We also help run the Nuclear Forensics Undergraduate Summer Program sponsored by DHS-DNDO (FY11 held at Washington State) and recruit potential students.

This year students conducted research on such diverse topics as: actinide (Np, U, Pu) isotopic fingerprinting, statistical modeling in nuclear forensics, actinide analysis for nuclear forensics, environmental radiochemistry, radiation detector materials development, coincidence counting methods, nuclear chemistry, and heavy element separations chemistry.

In addition to hands on training, students attend a weekly lecture series on topics applicable to the field of nuclear forensics (see Table 2). Speakers are experts from both within and external to LLNL. Speakers are able to discuss the importance of their work in the context of advances in the field of nuclear forensics.

Graduate students are invited to return for a second year at their mentor's discretion.

For the top graduate students in our program, we encourage the continuation of research collaboration between graduate student, faculty advisor and laboratory scientists. This year we hosted two students that were awarded a Nuclear Forensics Graduate Fellowship.

We use our summer program to create a successful pipeline of top quality students from universities across the U.S. Since 2002, 42 students have returned and/or conducted their graduate research at LLNL. Eleven have become postdoctoral fellows, and 7 have been hired as career scientists at LLNL. Two summer students have taken postdoc positions at other national labs. Three summer students have gone on to work at other national laboratories as staff scientists, and three have gone on to faculty positions in national security/nuclear forensics/radiochemistry.

A big factor in the success of this program is the dedication of the staff scientists who volunteer to mentor the summer students. In FY11, funding from the Nuclear Forensics Graduate Mentoring Program (sponsor: DNDO) helped to partially support the time staff took to teach the summer interns. Staff scientists we able to take the necessary time to develop an appropriate summer project, oversee the safety training and dedicate more time helping the interns maximize their productivity and scientific potential.

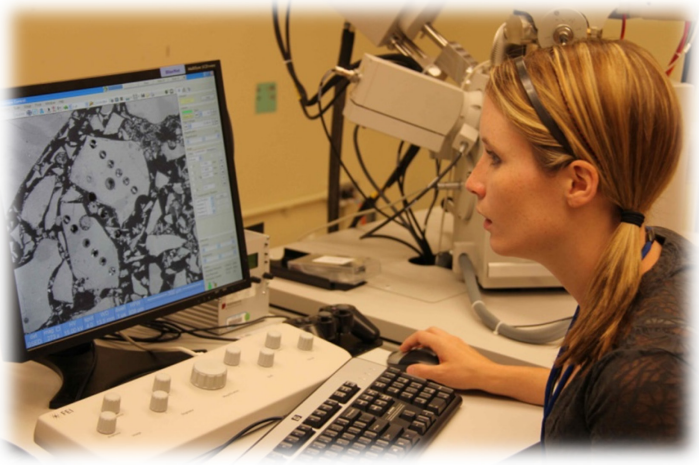


55
Monte Carlo Modeling of a Cavity Ion Source

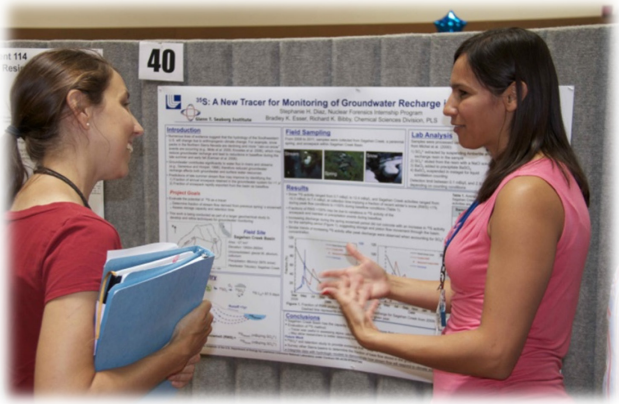
40
Field Sampling
Lab Analysis
Results
Conclusions

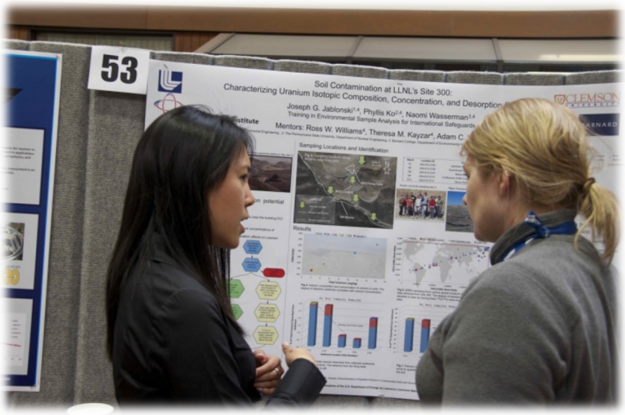
53
Soil Contamination at LLNL's Site 300:
Characterizing Uranium Isotopic Composition, Concentration, and Desorption
Sampling Locations and Identification
Results

## Table 1 Summer Students

| No. | Student | Major | University | Year |
|---|---|---|---|---|
| 1 | Perry Chodash | Nuclear Engineering | University of California, Berkeley | Grad |
| 2 | John Despotopulos | Chemistry | University of Nevada, Las Vegas | Grad |
| 3 | Stephanie Diaz | Earth Science | University of California Santa Barbara | Grad |
| 4 | Sandra Fernando | Geology | University of Michigan | Grad |
| 5 | Laurence Lewis | Nuclear Engineering | University of California, Berkeley | Grad |
| 6 | Anna Lindquist | Geophysics | University of Minnesota | Grad |
| 7 | Grayson Rich | Physics | University of North Carolina, Chapel Hill | Grad |
| 8 | Caleb Roecker | Nuclear Engineering | University of California, Berkeley | Senior Undergrad Started Grad school 9/11 |
| 9 | Christine Wallace | Civil Engineering and Geological Sciences | University of Notre Dame | Grad |
| 10 | Jennifer Wong | Environmental Engineering | Clemson University | Grad |
| 11 | Barbara Wang | Nuclear Engineering | University of California, Berkeley | Grad |

## Table 2 Seminar Schedule

| Date | Speaker | Topic |
|---|---|---|
| 6/23/11 | Brian Powell, Clemson University | Quantifying Actinide Behavior in Natural Systems for Nuclear Forensics Applications |
| 6/30/11 | Ken Moody, LLNL | Forensic Radiochemistry |
| 7/7/11 | Stephan Friedrich, LLNL | Detector Applications in National Security |
| 7/14/11 | James Begg, LLNL<br>Julie Gostic, LLNL<br>Brett Isselhardt, LLNL | Post-doctoral Research in Nuclear Forensics at LLNL |
| 7/21/11 | Rich Gostic<br>LLNL | Nuclear Forensics Case Study: Chemistry Supplies the Answers |
| 8/4/11 | Mona Dreicer, LLNL | Treaty Monitoring and Verification |

**Table 3 Student Projects and Mentors**

| Student | Mentor | Project |
|---|---|---|
| Perry Chodash* | Jason Burke | Nuclear Excitation Electron Transition decay in U-235 |
| John Despotopulos | Dawn Shaughnessy | Element 114 and 115 homologs using crown ether resins |
| Stephanie Diaz | Brad Esser | S-35 in snowmelt as an indicator of stream flow in alpine basins |
| Sandra Fernando | Mavrik Zavarin & Pihong Zhao | Transmission Electron Microscopy study of Np on goethite |
| Laurence Lewis | Ian Hutcheon | Monte Carlo modeling of cavity ion sources |
| Anna Lindquist | Kim Knight & Rich Gostic | Chemical variation in nuclear melt glass, Nevada Test Site |
| Grayson Rich | Kareem Kazkaz | Benchmarking digitizer data for gamma detection systems |
| Caleb Roecker | Nick Bowden | Using multiplexing for enhanced detector detection of anti-neutrinos |
| Christine Wallace | Rich Gostic & Kim Knight | Actinide identification in Nevada Test Site soils |
| Jennifer Wong | Mavrik Zavarin & Annie Kersting | Plutonium behavior on mineral surface in the presence of microbes |
| Barbara Wang** | Nick Scielzo | Cosmogenic Activation in neutrinoless double-beta decay |
| Mathew Snow** | Annie Kersting & Mavrik Zavarin | Np sorption to goethite |

* = nuclear nonproliferation international safeguards fellowship
**= Nuclear Forensics Graduate Fellows

# X-ray Fluorescence of NTS Soils for Matrix Characterization and Improvement of Gamma Spectroscopy Data

Christine M. Wallace[1], Richard Gostic[2], Kim Knight[2], Greg Spriggs[2], and Ian Hutcheon[2]
[1]University of Notre Dame, Department of Civil Engineering and Geological Sciences, Notre Dame, IN
[2]Lawrence Livermore National Laboratory, Physical and Life Sciences, Chemical Sciences Division, Livermore, CA

Glenn T. Seaborg Institute

Soils were collected at the Nevada Test Site from the site of a historical US surface test. Activity ratios calculated from gamma spectroscopy show sharply declining $^{241}Am/^{239}Pu$ and $^{137}Cs/^{239}Pu$ ratios in smaller gain sizes. The cause of this behavior is unknown. We hypothesized that the 59.5 keV photon from $^{241}Am$ was being attenuated by the matrix in samples with grain sizes below 500 µm.

## Isotope Ratios in Fallout Soil by γ Spectroscopy

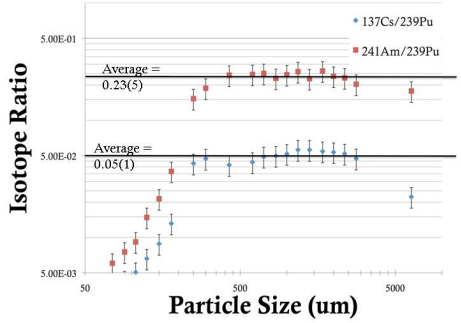


Samples were characterized via gamma spectroscopy using a planar HPGE detector. $^{241}Am:^{239}Pu$ and $^{137}Cs:^{239}Pu$ activity ratios were calculated from the gamma spectroscopy data for each size fraction. The results of this study indicated relatively constant $^{241}Am:^{239}Pu$ and $^{137}Cs:^{239}Pu$ for particles larger than 600µm, but a sharp decline in both ratios was evident in the smaller grain sizes.

## γ Spectroscopy of the 1250 µm Size Fraction

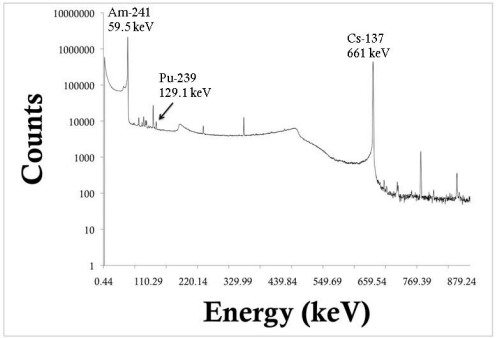



Bruker S8 Tiger XRF

To test the hypothesis that the soil matrix was causing differential attenuation of the 59.5 keV photon from $^{241}Am$ and/or the 661 keV photon from $^{137}Cs$ in the smaller size fractions, major and select trace element matrix characterization was carried out for each sample via X-ray fluorescence (XRF) wavelength dispersive analysis. Densities were measured for each soil size fraction volumetrically. Explicit density measurements were needed in order to carry out the attenuation calculations.

| Sample | Size (um) | Density (g/cm$^3$) |
|---|---|---|
| 3DW-30 | 600 | 0.61 |
| 3DW-40 | 425 | 0.59 |
| 3DW-50 | 300 | 1.02 |
| 3DW-60 | 250 | 1.11 |
| 3DW-80 | 180 | 1.31 |
| 3DW-100 | 150 | 1.32 |
| 3DW-120 | 125 | 1.31 |
| 3DW-140 | 106 | 1.32 |
| 3DW-170 | 90 | 1.36 |
| 3DW-200 | 75 | 1.37 |

XCOM

*NIST XCOM*

Mass attenuation coefficients were calculated using the online version of *NIST XCOM: Photon Cross Section Database*, and were subsequently used to generate corrected attenuation curves and re-calculate both ratios for each sample

## Sample 3DW-200 (75 um), XRF Results

| Formula | Concentration (%) | Error (%) |
|---|---|---|
| $SiO_2$ | 24.89 | 0.24 |
| CaO | 11.56 | 0.19 |
| $Al_2O_3$ | 4.19 | 0.63 |
| $K_2O$ | 2.14 | 0.41 |
| $Fe_2O_3$ | 2.02 | 0.25 |
| MgO | 1.42 | 1.13 |
| $TiO_2$ | 0.31 | 1.34 |
| $Na_2O$ | 0.23 | 6.75 |
| SrO | 0.12 | 0.68 |
| BaO | 0.11 | 4.91 |
| $P_2O_5$ | 0.06 | 5.19 |
| MnO | 0.06 | 1.87 |
| $SO_3$ | 0.03 | 7.41 |
| $Rb_2O$ | 0.03 | 1.97 |

Measured elemental concentrations show little variation from sample grain size to sample grain size. One example of elemental concentrations and errors is shown above. In order to verify that the XRF results are not dependent on grain size, a portion of sample 3DW-30 (600 um) was ball-milled for 10 minutes subsequent to the first XRF run. The sample was then measured again via XRF in order to verify the elemental composition.

## Elemental Composition of Soils as Determined by XRF

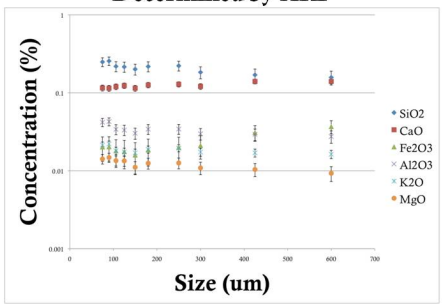


Correcting the ratios for matrix attenuation effects does not account for the decline in $^{241}Am$ and $^{137}Cs$ activities relative to $^{239}Pu$ as a function of grain size.

## Attenuation Calculation, 59.5 keV $^{241}Am$ Photon:

total attenuation (XCOM):

$\mu/\rho = 2.55E\text{-}01\ cm^2/g$

(attenuation)*(density):

$(\mu/\rho) * (\rho) = \mu = 3.50E\text{-}01\ cm^{-1}$

attenuation factor (%) = $I/I_o = e^{-\mu x}$

where x = sample thickness (cm)

$I/I_o = \exp[(-0.350\ cm^{-1})*(1\ cm)$ = **0.705**

## Attenuation by Photon Energy

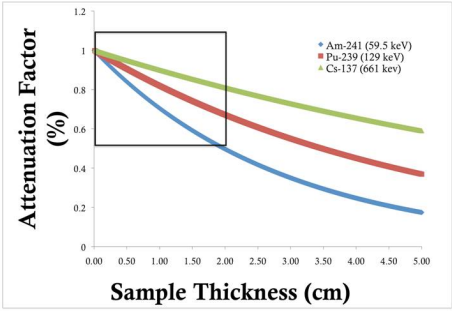


## Conclusions

We conclude that the depressed $^{241}Am/^{239}Pu$ and $^{137}Cs/^{239}Pu$ ratios at grain sizes below ~500 microns are not an artifact of sample preparation or matrix attenuation, but may instead be due to differences in chemistry between Am/Cs and Pu. This result was not anticipated for $^{241}Am/^{239}Pu$ because Am grows into the Pu matrix via decay of $^{241}Pu$, and was presumed to be rendered immobile in this matrix. Preferential leaching of $^{137}Cs$ is less surprising, because $Cs^{2+}$ does tend to be environmentally mobile. We can further test this through leaching experiments of larger soil size fractions.

This work performed under the auspices of the U.S. Department of Energy by Lawrence Livermore National Laboratory under Contract DE-AC52-07NA27344

LLNL-POST-491921

# Plutonium Contaminant Transport: Subsurface Mobilization by a Siderophore

Jennifer C. Wong

Jennifer C. Wong[1,2], Pihong Zhao[1], James Begg[1], Mavrik Zavarin[1], Annie Kersting[1], Brian A. Powell[2]

[1]Lawrence Livermore National Laboratory, Glenn T. Seaborg Institute, 7000 East Ave., Livermore, CA 94550; [2]Clemson University, Dept. Environmental Engineering & Earth Science, 342 Computer Ct., Anderson, SC 29625

## Abstract

The effect of desferrioxamine B (DFOB), a naturally occurring bacterial siderophore, on plutonium transport in goethite-containing sediments was examined. DFOB solutions were applied to goethite with pre-adsorbed plutonium in batch and flow experiments. In batch experiments conducted with 0.5 mgC/L DFOB, Pu desorption from goethite continued to occur after 35 days. More than 99% of Pu was removed from goethite in a stirred cell after 40 chamber volumes of 0.5 mgC/L DFOB solution was pumped through over 5 days. The breakthrough curve for a column packed with sediments from the Savannah River Site, USA (SRS) was comparable to that of a Pu(V) ligand-free system, indicating that Pu-DFOB complexes are highly mobile and can dramatically increase Pu transport rates.

## Background

- Knowledge of Pu mobility at sites such as the Savannah River Site (SRS) is required to assess risks associated with:
  - Release of Pu into the environment
  - Prediction of subsurface Pu transport
  - Design of remediation strategies

**Goal:**
**Study rate of DFOB-mediated Pu desorption from goethite, and implications for Pu transport.**

- As low molecular weight iron chelators[3], siderophores, such as DFOB, are expected to form soluble complexes with Pu, which has a similar electron density to iron[1].
- Batch sorption studies on gibbsite, show a large portion of Pu is not sorbed in the presence of DFOB compared to a ligand-free system[4].
- Column studies show retardation factors less than 5 for a ligand-free Pu(V) system[2].

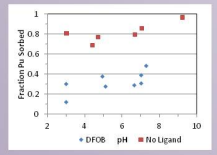


Figure 1. Fraction of Pu sorbed to Gibbsite after 7 days in the presence of 5 mg C/L and no ligand[4].

## Batch Experiment

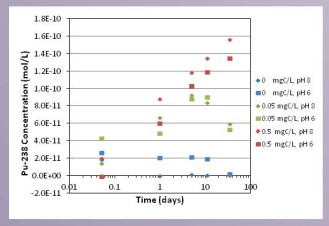


Figure 2. Pu was adsorbed to a 0.1 g/L goethite suspension for 2 days, then DFOB was added. DFOB at 0.5 mg C/L caused Pu to desorb over at least 35 days. The decrease in aqueous Pu after 11 days with 0.05 mg C/L DFOB may be due to microbial degradation of DFOB. With DFOB present, more Pu desorbed at pH 8 compared to pH 6, indicating that DFOB complexes more strongly with Pu when deprotonated. Without DFOB, virtually no Pu desorbed at pH 8.

## Stirred Flow-Cell

- Cell initially spiked with DFOB-free Pu & goethite solution
- DFOB background solution flowed throughout experiment

Parameters:
pH goal: 6
DFOB Concentration: 0.5 mg C/L
DFOB Loaded: Continuously
Chamber Volume: 20.2 mL
Contact Time: 53 min
Substrate: 0.1 g/L synthetic goethite suspension

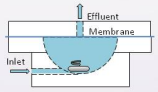


Figure 3. Experimental setup. A magnetic stir bar was placed in the teflon flow-cell.

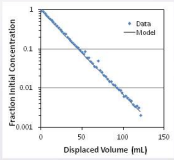


Figure 4. A run conducted with tritium tracer indicates good mixing and flow. A model fit yields effective chamber volume.

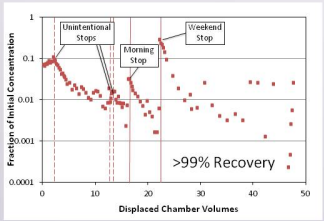


Figure 5. Pu in flow-cell effluent. More than 99% of Pu was recovered. Stop flow events were used to gauge desorption rates. A few unintentional stop flow events occurred due to pump malfunctions. The initial increase in Pu occurs while the first, DFOB-free chamber volume is pumped out.

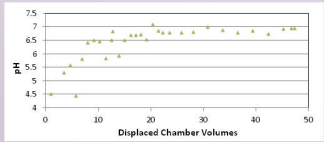


Figure 6. The pH of the effluent increased during the first 15 chamber volumes. This could be due to off-gassing of $CO_2$ from the influent reservoir or buffering of the goethite.


Figure 7. SEM images of goethite crystals (A) before and (B,C) after the flow-cell experiment. There do not appear to be any signs of significant iron dissolution or physical wear from stirring. The round-looking attachments in (C) could be an unidentified contaminant.

## Sediment Column

- One pore volume of Pu & DFOB was loaded
- DFOB-free background solution was flowed continuously

Parameters:
pH: 5
DFOB Concentration: 50 mg C/L
Pu & DFOB Loaded: 6.2 mL
Pore Volume: 6.3 mL
Contact Time: 1 hour
Substrate: SRS sediment (goethite coated sand)

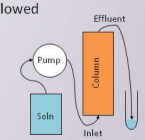


Figure 8. Sediment column set up. Column length is 8.3 cm.

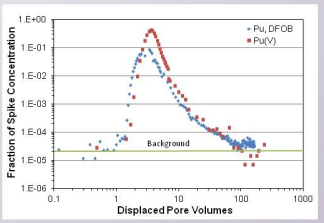


Figure 9. The breakthrough curve of the DFOB column compared to the breakthrough of ligand-free Pu(V). The similar shape indicates that mobile Pu, most likely in the form of Pu-DFOB complexes, behaves the similarly to uncomplexed Pu(V).

| Column | Retardation Factor | Effluent Recovery | Soil Digestion Recovery |
|---|---|---|---|
| Pu, DFOB | 5.9 | 5.5% | 70.1% |
| Pu(V)[2] | 4.4 | 75.6% | 6.5% |

Table 1. Although the retardation factors for the DFOB column and the Pu (V) column are similar, only a small portion of Pu in the DFOB column is eluted because the background solution is ligand-free. The Pu uncomplexed with DFOB adsorbs to the sediment.

## Conclusions

- DFOB can desorb Pu from goethite slowly (over a period >35 days)
- Sorption to goethite is very reversible (>99% removal under flow conditions).
- SEM images do not show significant dissolution of the iron matrix.
- In SRS sediments, Pu-DFOB complexes were as mobile as uncomplexed Pu (V).
- Implications
  - The presence of siderophores (such as those produced by microorganisms and plants) has the potential to desorb and mobilize subsurface Pu.
- Future Work
  - Flow-cell experiments with more controlled pH at 6 and 8
  - Apply 1-D reactive transport model to determine sorption, desorption, and aqueous complexation rate constants.
  - More SEM images to identify unidentified attachments, and whether microorganisms are present.

This work performed under the auspices of the U.S. Department of Energy by Lawrence Livermore National Laboratory under Contract DE-AC52-07NA27344.
This work was supported by the Subsurface Biogeochemical Research Program of the U.S. Department of Energy's Office of Biological and Environmental Research.

1. Morss, L. R., Edelstein, N. M., & Fuger, J. (Eds.). (2006). Chapter 7: Plutonium. In *The Chemistry of the Actinide and Transactinide Elements* (3rd ed., Vol. 1, pp. 813-1264). Dordrecht, Netherlands: Springer.
2. Powell, B.A.; Fjeld, R.A.; Coates, J.T.; Kaplan, D.I.; Serkiz, S.M., Plutonium oxidation state geochemistry in the SRS subsurface environment. WSRC-TR-2003-00035. SRNL 2002.
3. Powell, P.E., Cline, G. R., Reid, C. P., & Szaniszlo, P. J. (1980, October 30). Occurrence of hydroxamate siderophore iron chelators in soils. *Nature, 287*, 833-834.
4. Simpkins, L.; Unpublished.

LLNL-POST-492391

# Feelin' hot, hot, hot!

Anna Lindquist[1], Kim Knight[2], Rich Gostic[2], Gary Stone[2], Ian Hutcheon[2], and Greg Spriggs[2]
[1]University of Minnesota, Department of Earth Sciences, Minneapolis, MN
[2]Lawrence Livermore National Laboratory, Physical and Life Sciences, Chemical Sciences Division, Livermore, CA

Glenn T. Seaborg Institute

*Are the glass spheres formed following a nuclear blast homogenous? What can autoradiography reveal about their internal structure?*

## Is the Distribution of Radioactivity in Fallout Uniform?

Following an above ground nuclear explosion, materials that have been super-heated cool and condense, forming fallout debris. Glassy materials are a commonly observed component of fallout debris, and may capture and preserve information about the starting materials, fissioned materials and products, and the environment of the explosion. It has been hypothesized that the radioactive nuclides captured in fallout debris are concentrated along the outer edges of the glassy debris [1,2]. Alternately, other theories suggest that the radionuclides should be well-mixed and homogenously distributed throughout the glassy debris [1,2]. Previously, radiography has been useful in investigating whether radioactivity was dispersed throughout the sample or concentrated in specific areas [1] soon after formation. We utilized contact autoradiography to determine which of these hypotheses is correct decades later, and whether or not the distribution of radionuclides within fallout may still provide clues as to the chemistry and physics behind the formation of fallout.

We looked at fallout debris glass from two different US nuclear tests, one from a Pu-based fuel (WS) and one from a U-based fuel (NT). Contact autoradiography enables us image how the radioactivity is distributed within a sample. The radiographic images are formed primarily by $\beta^-$ radiation. This is extremely useful because $\beta^-$ emitters (like $^{90}Sr$) can be difficult to see using gamma spectroscopy and other conventional methods, yet are among the primary nuclides produced in fission. Autoradiography and scanning electron microscopy (SEM) were used in concert to investigate the degree of homogeneity or heterogeneity in these samples.


laboratory work

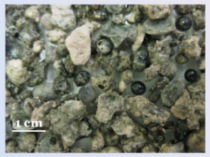

mixed fallout debris

radiographic setup

## Imaging Fallout Debris

Select glass spheres from fallout debris were set into epoxy and polished flat. Optical images of these samples show a green to brown coloration, and circular cross section. Backscattered electron (BSE) images were taken on an FEI Inspect F SEM. BSE images show relative compositional differences. Areas with higher Z elements reflect more electrons, so they appear brighter, while areas with lower Z elements appear darker. We used BSE images to help determine the compositional structure of these glasses.

For this study, all radiographic imaging was recorded on SR (super resolution) or TR (tritium) image plates. The IPs were placed in a tray within the the light-blocking tent (above). Samples were placed against the image plates and weighted slightly to stability and contact with the plates. Arm holes in tent allowed manipulation of samples while still within the tent, if necessary. Depending on activity, polished fallout spheres were left for 18 to 90 hours. It was important to scan the image plates soon after the exposure time because 50% of the signal fades within 3.5 hours [3]. Spatial resolution on this scanner was set at ~50 µm.

***Optical Imaging***
Visible light images showing structures on surfaces and within samples.

***Scanning Electron Microscopy (SEM)***
Backscattered electron images showing compositional variation

***Autoradiography***
Qualitative images formed by emitted beta radiation showing radionuclide distribution.

No activity — High activity

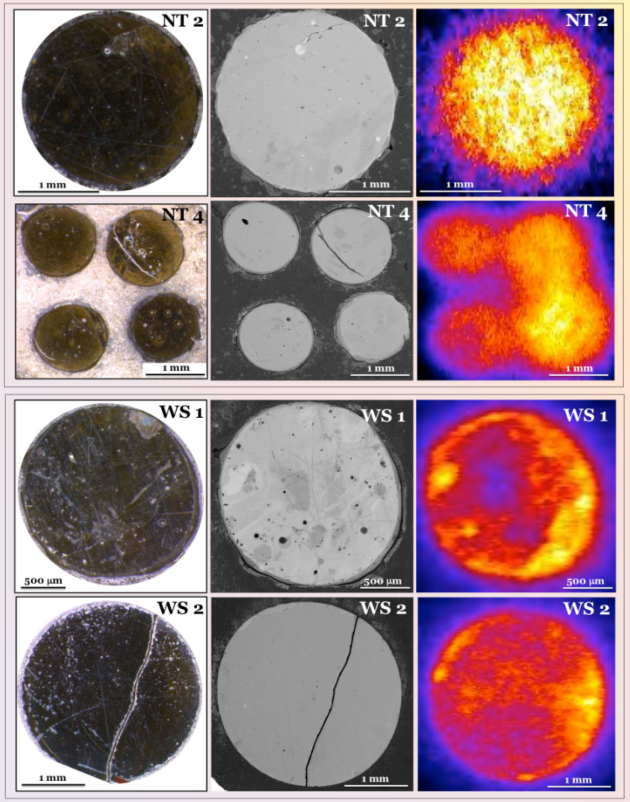


Images of NT and WS spheres. SEM images show chemical inhomogeneity in some samples (WS1), and uniform composition in others (WS2). Autoradiographic images from some samples show strong correlations with compositional variations observed in SEM images (WS1). Other samples show inhomogeneity in radionuclide without first-order chemical variation (WS2).

*For NT2 radiographic images may not have the same orientation as optical, SEM images.

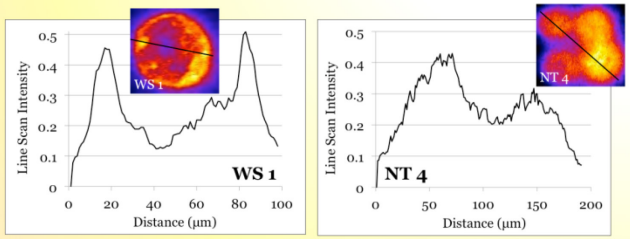


Line scans across NT 4 and WS 1 to illustrate the variation in intensity across the radiography images. Some samples show the highest concentration at the rims (here, WS1), while others (here, NT4) show the highest concentrations in the centers.

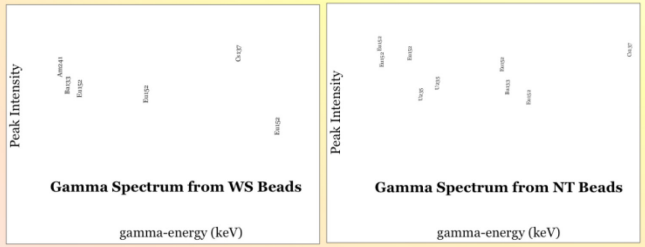


Gamma spectra for NT and WS samples illustrate the main fission fuel and activation peaks present in the samples. $\beta^-$ emitters, however, such as those imaged by radiography cannot be detected by this method, but may (or may not!) follow similar distributions.

## Concluding Thoughts

We find evidence for heterogeneity with respect to the distribution of radionuclides in all of the samples examine, but to varying degrees. we see that the glass beads from the two tests show distinct internal structures, and that the distribution of material within glassy fallout is not always homogenous, and varies within and between tests. Some regions within a debris sample may contain higher concentrations of materials directly related to the explosion, while other regions may reflect the surrounding environment. Further work will be necessary to determine the causes of these differences. It will also prove useful to correlate intensity in autoradiographic images with activity, quantitatively. Most importantly, our work demonstrates that autoradiography is a relatively simple and rapid technique that can be used to investigate the dispersion of radioactive material within a sample and to identify regions of interest for further study.

**References**

1) Adams, C. E., N. H. Farlow, W. R. Schell (1960), The compositions, structures, and origins of radioactive fall-out particles, *Geochemica et Cosmochimica Acta, 18*, pp. 42-56.
2) Glasstone, S. and P.J. Dolan (1977), *The Effects of Nuclear Weapons*, United States Dept. of Defense and Dept. of Energy, 653 pp.
3) Maddox, B. R., H. S. Park, B. A. Remington, N. Isumi, S. Chen, C. Chen, G. Kimminau, Z. Ali, M. J. Haugh, Q. Ma (2011), High-energy x-ray backlighter spectrum measurements using calibrated image plates, *Review of Scientific Instruments*, *82*, doi:10.1063/1.3531979.

This work performed under the auspices of the U.S. Department of Energy by Lawrence Livermore National Laboratory under Contract DE-AC52-07NA27344

LLNL-POST-xxxxxx

# Extraction Chromatographic Studies of Element 114 and 115 Homologs Using Crown Ether Based Resins

John Despotopulos[1], Julie Gostic[2], Evgeny Tereshatov[2], Roger Henderson[2], Ken Moody[2], Dawn Shaughnessy[2], Ralf Sudowe[1]

[1]University of Nevada – Las Vegas, [2]Chemical Sciences Division – Lawrence Livermore National Laboratory

LLNL-POST-492275

## INTRODUCTION AND MOTIVATION

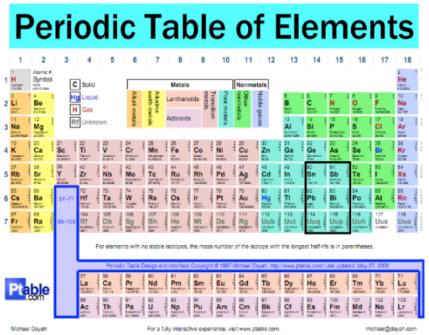


Recent studies of the chemical behavior of element 112 and 114 in the gas phase together with the discovery of isotopes with suitable half-lives have spurred a renewed interest in the development of suitable chemical systems to study the solution chemistry of elements with Z ≥ 114 [1-2]. Due to the short half-lives of the transactinide elements, fast and efficient separations are necessary so that the chemical properties of these elements can be compared to those of their lighter homologs. Separations based on extraction chromatography resins show promise for achieving the required short separation times, high yields, and high separation factors that are required for transactinide studies. The adsorption of Pb and Sn, the lighter homologs of element 114, on Eichrom's Pb extraction chromatographic resin has been investigated from various acid matrices to evaluate the suitability of these systems for the study of element 114. Similarly, Bi and Sb, the lighter homologs of element 115, have been used to evaluate these systems for the investigation of element 115.

## TRANSACTINIDE CHEMISTRY CHALLENGES

- Low production rates, with only a few atoms produced over the entire cycle.
- Short lifetimes, ranging from $10^{-9}$ seconds to a few hours.
- Chemical system must be reliable, robust, fast, and extremely efficient for ultra-trace applications (Automation required).

## PROJECT GOALS

- Continue research aimed at the production of transactinide elements.
- Develop a chemical system for separating the homologs and pseudo-homologs of element 114 and 115 (Sn, Pb and Sb, Bi respectively).
- Separation scheme must give knowledge of the chemical form of the homologs and pseudo-homologs during the separation procedure, to allow extrapolation of the transactinide elements chemical properties.
- Chemical system must be automatable.

Physical and Life Sciences Directorate

## EXTRACTION CHROMATOGRAPHY

Extraction chromatography grants the selectivity of liquid-liquid extraction with the ease of running a column. An extractant is coated onto an inert support, and serves as the stationary phase. The mobile phase, for the purpose of this experiment, consists of an acid such as hydrochloric or nitric. The number of free column volumes to reach peak maximum for a given elution is given by a factor k':

$$k' = (D_w)\left(\frac{d_{extr}}{0.4}\right)\left(\frac{v_s}{v_m}\right)$$

Where $\left(\frac{v_s}{v_m}\right)$ is the resin factor, $d_{extr}$ is the density of extractant, 0.4 is the ratio of extractant loading, and $D_w$ is the distribution factor given by:

$$D_w = \left(\frac{A_o - A_s}{A_s}\right)\left(\frac{mL}{g}\right)$$

Where $A_o - A_s$ is the activity on the resin of known mass, g, and $A_s$ is the activity in a known volume, mL [3].

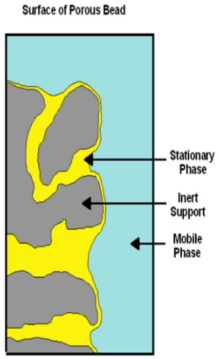


E. P. Horwitz, "Extraction Chromatography of Actinides and Selected Fission Products: Principles and Achievement of Selectivity," [Online], Eichrom Technologies Inc., http://www.eichrom.com/products/extraction.cfm (Accessed: 7/30/2011).

## EICHROM'S Pb RESIN

Di-t-butylcyclohexano-18-crown-6 extractant

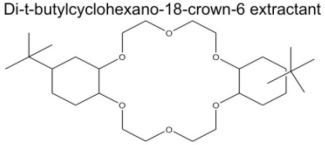

- 0.75M di-t-butylcyclohexano-18-crown-6.
- Isodecanol solvent.
- Available as free resin.
- Available as 2mL pre-packed cartridges.
- $\left(\frac{v_s}{v_m}\right)$ = 0.24.
- $d_{extr}$ = 0.917 g/mL.
- Fast Kinetics.
- High ionic radius based selectivity.
- Stable and robust extractant.

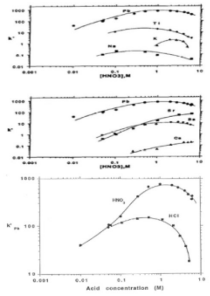


E. P. Horwitz, M. L. Dietz, S. Rhoads, C. Felinto, N. H. Gale, and J. Houghton, "A lead-selective extraction chromatographic resin and its application to the isolation of lead from geological samples," Analytical Chemica Acta 292, 263-273 (1994).

This work was performed under the auspices of the U.S. Department of Energy by Lawrence Livermore National Laboratory under Contract DE-AC52-07NA27344. This work was funded by the Laboratory Directed Research and Development Program at LLNL under project tracking code 11-ERD-011.

## EXPERIMENTAL PROCEDURE

Batch Studies: optimize matrix composition (either [HCl] or [$HNO_3$]).

-Stable:
- 5 mL solution with 200 ppb Bi and Sb or Pb and Sn, aliquot diluted and analyzed by ICP-MS.
- Remaining solution contacted with 30-50 mg Eichrom Pb resin, one hour equilibration time.
- Centrifuged and supernate diluted for ICP-MS analysis.

-Active:
- 10-20 mg Eichrom Pb resin added to 1 mL solution (with either Pb, Sn, Ge or Sb, Bi isotopes), two hour equilibration time.
- Activity verified by HPGe gamma spectroscopy.

## RESULTS

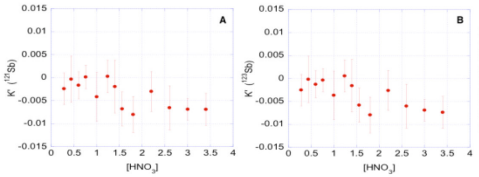


**Figures A-C.** The batch uptake (k') of the selected ions as a function of nitric acid media on Pb resin (50-100 μm) with a 1 hour equilibration time.

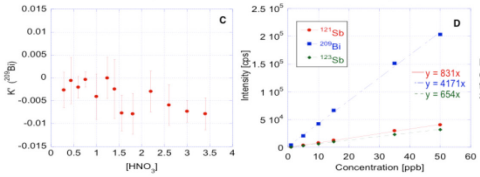


**Figure D.** ICP-MS calibration curves for $^{121,123}Sb$, and $^{209}Bi$.

## CONCLUSIONS AND FUTURE WORK

Initial batch results indicate Eichrom's Pb resin is not suitable for separations of Bi and Sb. Future work will seek to: perform studies using Pb, Bi, Sn, and Sb radioisotopes; establish best acid matrices and elution concentrations to perform Pb, Sn and Bi, Sb separations; determine the chemical form of the homologs during separation; and expand separation procedures to include the pseudo-homologs, Hg, Cd and Tl, In for element 114 and 115 respectively.

Separation schemes will be evaluated, on-line, with short-lived homologs produced at LLNL CAMS facility.

## REFERENCES

[1] R. Eichler *et al.*, "Chemical characterization of element 112," Nature 447, 72-75 (2007).
[2] R. Eichler *et al.*, "Indication for a volatile element 114," Radiochim. Acta 98, 133-139 (2010).
[3] E. P. Horwitz, R. Chiarizia, and M. L. Dietz, "A Novel Strontium Selective Extraction Chromatographic Resin," Solvent Extr. Ion Extr. 10, 313-336 (1992).

# Temporal Multiplexing for Position Measurement and Correction in Long Muon Veto Paddles

Glenn T. Seaborg Institute

**Caleb Roecker**
*Purdue University*
*Nuclear Forensics Internship Program*

**Nathaniel Bowden and Tim Classen**
*Lawrence Livermore National Laboratory*

## Long Muon Veto Paddle

The antineutrino detector comprises a liquid scintillator (Gd doped) volume readout from two ends. This is surrounded by a mineral oil buffer, a water shield, and plastic scintillator paddles to reject cosmic ray muons.

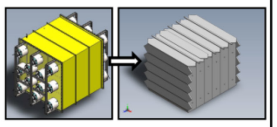

$$\bar{\nu}_e + p \rightarrow n + e^+$$

An antineutrino entering the detector will occasionally interact via inverse beta decay. The positron quickly combines with an electron producing two photons. The neutron thermalizes and is absorbed by $^{157}$Gd, producing a shower of gamma rays. Both signals must be observed to record an event.

Muons can produce neutrons in the detector, potentially causing false positives, compelling the installation of a muon veto system.

$$\mu + A \rightarrow \mu + A^* + n$$

## Experimental Setup

Two types of muon paddles are used: Fish Tail (top) and Square (bottom) each with two photomultiplier tubes (PMTs). The experimental setup is shown with a muon telescope used to select events where a muons passes through a well defined 1'x1'area. PMT signal amplitudes were recorded as a function of position using this method.

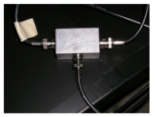

A delay cable is introduced on one of the PMTs creating a temporal offset. This allows the two PMT signals to be analyzed using a single readout channel (multiplexing).

## Data Acquisition

The original PMTs signals can be extracted from the multiplexed signal by applying 3 integration regions around the hardware trigger. This allows either PMT signal to trigger the acquisition, yielding a wide dynamic range. A pedestal integration region is also used to subtract the signal baseline.

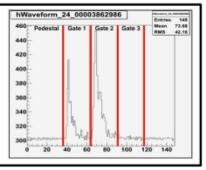


The 2 PMT signals obtained via multiplexing can be used to estimate the interaction position, and there correct for position dependent light collection from the paddles. This in turn results in improved energy resolution and gamma ray rejection.

$$PMT \propto \exp(-\beta x) \propto E_{individual}$$

$$x = (1/2\beta)\ln(PMT2/PMT1)$$

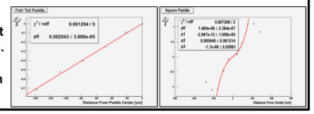


## Multiplexing Benefits

The cost, size and complexity of the detector system is reduced by using a delay cable instead of a second readout channel, while preserving full information about an event. For example, the cost per readout channel is ~$1000, while the cost per cable is ~ $50. There are ~60 muon veto PMTs.

Gain matching can be performed during post-processing allowing for non-identical PMTs to be on the same paddle and reducing the hardware configuration time.

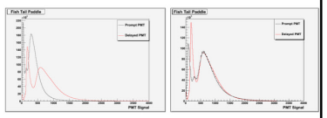


## Improved Gamma Rejection

Using multiplexing and implementing a post-process gain matching reduces the background events mischaracterized as muons. Further background rejection is possible by correcting for position, assuming light is exponentially attenuated and that a better estimate of the energy is

$$E_{total} \propto \sqrt{PMT1 \cdot PMT2},$$

instead of

$$E_{total} \propto PMT1 + PMT2.$$

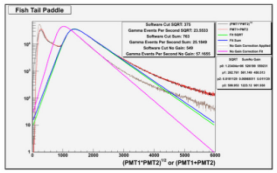


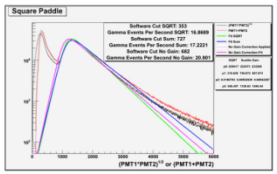


## Position Sensitive Veto

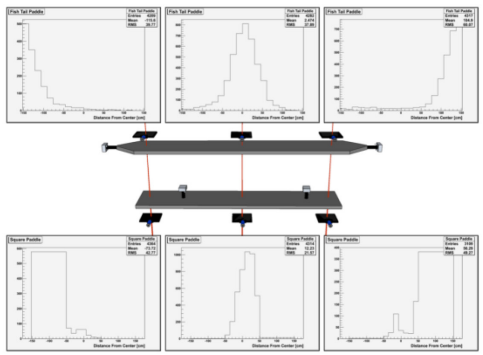


## Conclusions

1. Muon background rejection is essential to an antineutrino detector.
2. Multiplexing decreases the cost of the detector while preserving the data acquired.
3. Gain matching of PMTs in post processing reduces hardware matching requirements and improves background rejection.
4. Appling a position correction in the energy estimation of events further improves background rejection.
5. Coarse position reconstruction is achievable. The Fish Tail paddles have better spatial resolution across the whole paddle than the Square paddles.

Lawrence Livermore National Laboratory

LLNL-POST-491823
This work was performed under the auspices of the U.S. Department of Energy by Lawrence Livermore National Laboratory in part under Contract W-7405-Eng-48 and in part under Contract DE-AC52-07NA27344.

# Cosmogenic Activation in the Neutrinoless Double-beta Decay Experiment CUORE


Barbara S. Wang[1], Eric B. Norman[1], Nicholas D. Scielzo[2], Steven A. Wender[3], Matthew Devlin[3], Alan R. Smith[4]

[1]University of California, Berkeley; [2]Lawrence Livermore National Laboratory; [3]Los Alamos National Laboratory; [4]Lawrence Berkeley National Laboratory



**Abstract:** CUORE (Cryogenic Underground Observatory for Rare Events) is an experiment that will search for neutrinoless double-beta (0νββ) decay. The CUORE detector is an array of 988 high-resolution, low-background $TeO_2$ bolometers operated at cryogenic temperatures. All sources of background that can obscure the 0νββ decay signature must be well-understood. One of these sources is cosmogenic activation of the bolometers. A reliable estimation of this background is essential but difficult to obtain because of the lack of cross-section data. Thus, cross-section measurements have been carried out at LANSCE (Los Alamos Neutron Science Center).


## Introduction

**Double-beta Decay:**

**2νββ:** $(A,Z) \rightarrow (A,Z+2) + 2e^- + 2\bar{\nu}_e$
Allowed by Standard Model

**0νββ:** $(A,Z) \rightarrow (A,Z+2) + 2e^-$
Not allowed by Standard Model

- Want to answer:
  - Is ν Majorana or Dirac particle?
  - What is neutrino mass scale and hierarchy?
  - Is lepton number conserved?

**CUORE Detector:**

- Located underground at Gran Sasso National Laboratory in Italy
- Data-taking starts 2014
- 988 $TeO_2$ bolometers at 10 mK (natural Te used)
- 0νββ decay reaction: $^{130}Te \rightarrow {}^{130}Xe + 2e^-$
  (Decay energy = 2527 keV. Isotopic abundance of $^{130}Te$ = 34%)

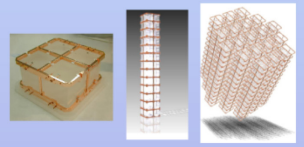

**Bolometer:**

- **Absorber:** 5x5x5 $cm^3$ $TeO_2$ crystal
- **Thermal sensor:** Neutron transmutation doped (NTD) germanium semiconductor thermistor
- **Heat sink:** Copper frame at 10 mK

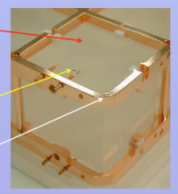

Particle interaction in **absorber** deposits energy ΔE → **Thermal sensor** measures temperature rise ΔT = ΔE/C → Absorber returns to **heat sink** temperature

**Double-beta Decay Signatures in CUORE:**

- ΔE = energy deposition in detector
- Q = decay energy
- **2νββ decay signature:** energy continuum up to Q
- **0νββ decay signature:** peak at Q (2527 keV in CUORE)

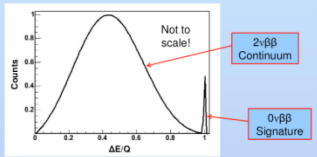


**Background Events:**

- An event that is not 0νββ decay and can obscure the 0νββ decay peak is considered background
- Need extremely low background in region around 2527 keV (gray in the figure)
- CUORE's goal background at 2527 keV: 0.001 – 0.01 counts/keV/kg/year
- Thus, all sources of background must be well-understood!!

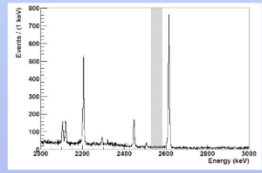


- Background due to cosmogenic activation of the $TeO_2$ bolometers highly uncharacterized

**Cosmogenic Activation in CUORE:**

- $TeO_2$ crystals grown in Shanghai, China and shipped by boat to Gran Sasso, Italy, where they are stored underground
- Each crystal spends ~ 3 months above ground at sea-level
- Sea-level cosmic ray interactions with $TeO_2$ produce long-lived radioisotopes, i.e., cosmogenic activation
- Several of these isotopes can obscure 0νββ decay peak at 2527 keV. Examples:

| Isotope | Half-life | Decay Energy (keV) | Decay Mode |
|---|---|---|---|
| Co-60 | 5.271 y | 2824 | β- |
| Sb-124 | 60.20 d | 2905 | β- |
| Co-56 | 77.27 d | 3544, 4566 | β+, EC |
| Y-88 | 106.7 d | 2601, 3623 | β+, EC |
| Ag-110m | 249.8 d | 3010 | β- |

- Reliable estimation of cosmogenic activation background needed. Difficult to obtain because of lack of accurate cross-sections.

## Methods and Results

At sea-level, most cosmogenic activation due to interactions with cosmic ray neutrons

**Cross-section Measurements at LANSCE (December 2-4, 2010):**

- Irradiated $TeO_2$ targets with 30°-left neutron beam at LANSCE. This spectrum mimics cosmic ray neutron spectrum at sea-level.
- **Targets:**
  - Nine 1x1x1 $cm^3$ $TeO_2$
  - One 5x5x5 $cm^3$ $TeO_2$
  - One 5x5x0.1 $cm^3$ $TeO_2$
  - One 5x5x0.64 $cm^3$ Al
  - One 5x5x0.64 $cm^3$ Polyethylene
- **Irradiation time:** 46.62 h
- **Source-target distance:** 26.47 m
- **Beam-spot diameter at target:** 11.58 cm

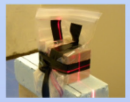

- **Schematic of experimental setup:**

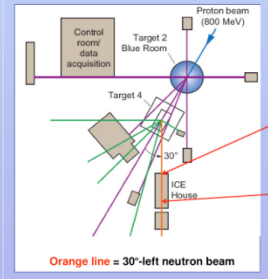


U-238 fission ionization used to measure neutron spectrum

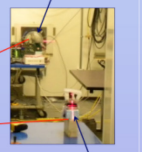

Targets

**LANSCE spectrum compared with cosmic ray neutron spectrum at sea-level:**

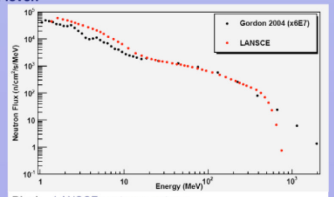


**Black** = LANSCE neutron spectrum
**Red** = Sea-level cosmic ray spectrum measured by Gordon et al. (Multiplied by $6 \times 10^7$ in plot)

**Subsequent Gamma-counting:**

- To obtain cross-sections for producing each isotope, nine 1x1x1 $cm^3$ $TeO_2$ crystals placed in front of HPGe detector


| Isotope | | Half-life |
|---|---|---|
| 17 d after irrad. | 170 days after irrad. | |
| Sb-120m1 | | 5.76 d |
| Sb-122 | | 2.72 d |
| Sb-124 | Sb-124 | 60.20 d |
| Sb-125 | Sb-125 | 2.758 y |
| Sb-126 | | 12.4 d |
| Sb-127 | | 3.84 d |
| Te-119m1 | | 4.69 d |
| Te-121 | Te-121 | 16.8 d |
| Te-121m1 | Te-121m1 | 154 d |
| Te-123m1 | Te-123m1 | 119.7 d |
| Te-127m1 | Te-127m1 | 109 d |
| Te-129m1 | Te-129m1 | 33.6 d |
| In-111 | | 2.805 d |
| Ag-105 | Ag-105 | 41.3 d |
| I-131 | | 8.020 d |
| Be-7 | Be-7 | 53.3 d |
| | Ag-110m | 249.8 d |

Note about table:
Blue = Short-lived isotopes
Red = Long-lived isotopes

**Cross-section Calculations:**

$$\bar{\sigma} = \frac{\lambda C_\gamma}{\varepsilon_\gamma B_\gamma \left[\exp(-\lambda t_{start}) - \exp(-\lambda t_{end})\right]\left[1-\exp(-\lambda t_{irrad})\right] N \int \varphi_{LANSCE}(E)\, dE}$$

Absolute peak efficiency is only unknown variable in equation

$\lambda$ = Decay constant of nuclide  $C_\gamma$ = Number of counts in $\gamma$ peak of interest  $\varepsilon_\gamma$ = Absolute peak efficiency  $B_\gamma$ = Branching ratio
$t_{start}$ = Start time of counting relative to the end of irradiation  $t_{end}$ = End time of counting relative to the end of irradiation
$t_{irrad}$ = Irradiation time  $N$ = Number of target atoms  $\varphi_{LANSCE}(E)$ = LANSCE neutron flux in n/MeV/cm²/s

**Absolute peak efficiency estimation:**

- Eu-152 calibration source placed in various positions
- Efficiency curve obtained for each position
- Absolute peak efficiency obtained by averaging over all curves

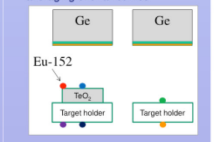


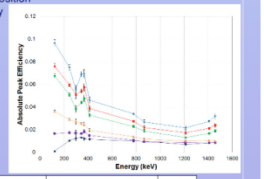


**Cross-sections of long-lived isotopes:**

Red = Can obscure 0νββ decay peak at 2527 keV

| Isotope | Half-life | Cross-section (mb) | +/- |
|---|---|---|---|
| Sb-124 | 60.2 d | 8.51 | 3.13 |
| Sb-125 | 2.758 y | 9.97 | 2.76 |
| Ag-105 | 41.3 d | 0.354 | 0.083 |
| Ag-110m | 249.8 | 0.128 | 0.052 |
| Be-7 | 53.3 d | 0.736 | 0.227 |

**Current and Future Work:**

- Currently using Geant4 to better characterize absolute peak efficiency
- Will perform second longer irradiation at LANSCE. Higher neutron fluence will allow for the measurement of longer-lived isotopes as well as smaller cross-sections.
- Will use cross-sections to estimate cosmogenic activation background present in CUORE


This work performed under the auspices of the U.S. Department of Energy by Lawrence Livermore National Laboratory under Contract DE-AC52-07NA27344.

IM Review Number: 503879, Release Number: LLNL-POST-492794

# Monte Carlo Modeling of a Cavity Ion Source

*Designing a more efficient ion source for mass spectrometry*

Laurence A. Lewis[1,2], Lars E. Borg[2], Ian D. Hutcheon[2]

[1] *University of California, Berkeley, Department of Nuclear Engineering*

[2] *Chemical Sciences Division, Glenn T. Seaborg Institute, Lawrence Livermore National Laboratory*

Glenn T. Seaborg Institute

## Goal: Model a cavity ion source to understand how the cavity's geometry and extraction potential affect ionization efficiency

## Overview: Greater ionization efficiency equals greater sensitivity.

Mass spectrometry is a powerful analytical tool in many disciplines, such as nuclear forensics and geochemistry. Isotope ratios can reveal insights into a sample's origin, age and history. **However, researchers are limited by the spectrometer's sensitivity, which is crucial in studies where samples contain low concentrations of the elements of interest.**

**Greater sensitivity will allow analyses of trace isotopes and elements simply not accessible by current techniques. To increase sensitivity we need more efficient ion sources.** Currently, thermal ionization mass spectrometers (TIMS) ionize material with <1% efficiency because most of the sample evaporates before ionizing (see Filament figure). Thus, most of the sample is lost before it even enters the mass spectrometer.

The cavity ion source (CIS) is an alternative to filaments. In contrast to flat filaments, the CIS is a hollowed Re rod (see CIS figure). The CIS ionizes elements with much higher efficiency than TIMS filaments, while using the same ionization mechanism (thermal ionization). Efficiency scales linearly with sensitivity, which would allow researchers to use smaller samples and detect elements present in lower concentrations.

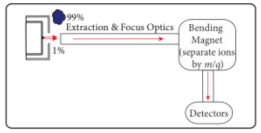


*Typical TIMS instrument*

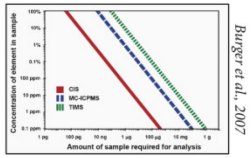


*Higher ionization efficiency enables analysis of smaller samples*

Burger et al., 2007

**The subject of this work is to design a CIS that optimizes ionization efficiency. This study models a CIS to determine how the ionization efficiency depends on the cavity's length, radius and extraction potential (the voltage placed between the CIS and an electrode to accelerate positive ions out of the cavity).**

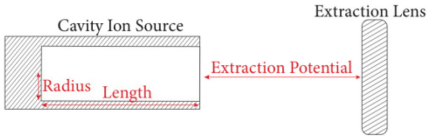


## Filament Ion Source

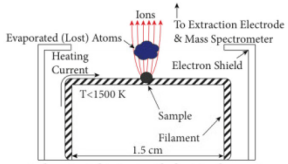


*Evaporated material is instantly lost to the environment.*

## Theory

The CIS and filaments ionize material the same way: thermal ionization. The Saha-Langmuir equation (α) is used to determine the probability of ionization or recombination.

$$\alpha = \exp[(\phi - E_i)/k_B T]$$

$\phi$: *work function of CIS*
$E_i$: *1st ionization energy of sample*
T: *temperature*

## Methods

SIMION 7.0 was used to model the cavity. Users define electrodes and SIMION calculates the velocity of ions through the resulting electric and magnetic fields. The model assumes a uranium sample load ($E_i$=6.2 eV) into a carburized rhenium cavity ($\phi$=5.3 eV) held at 2750 K. How atoms ionize, recombine and diffuse through the cavity is shown in *The Life of an Atom in the CIS.*

## Cavity Ion Sources in the Wild

*Duan et al., 1999*

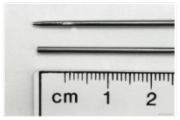


3.8%

*Riciputi et al., 2003*

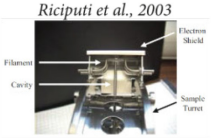


6.2%

*Zhai et al., 2011*


3-7%

Ionization Efficiency for Uranium Samples

## Cavity Ion Source

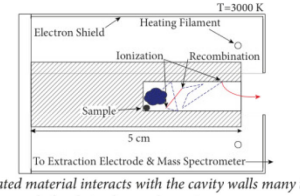


*Evaporated material interacts with the cavity walls many times before being lost to the environment.*

## The Life of an Atom in the CIS

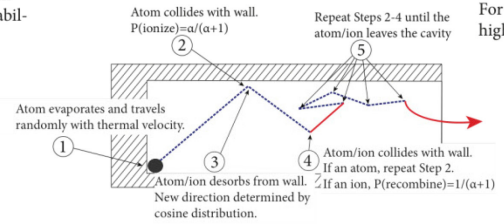


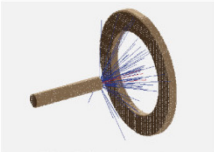

*The CIS in SIMION*

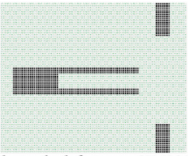

*Electrode defining in SIMION*

## Results: Wider cavities & larger extraction potentials increase the CIS efficiency.

For cavities of constant length,the widest cavity with the highest extraction potential performs best.

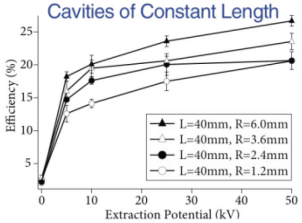


For cavities of constant radius, the cavity of intermediate length with the highest extraction potential performs best.

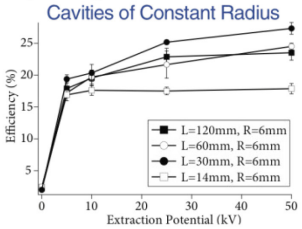


## Conclusion: The CIS can lower detection limits and increase sensitivity.

The cavity's efficiency is not strongly dependent on cavity dimensions or extraction potential (as long as there is one). However, wider radii and higher extraction potentials increase the efficiency because they allow the extraction field to penetrate deeper into the cavity, extracting ions as they form.

The CIS ionizes material far more efficiently than typical filaments (by >10 times). This leads to a commensurate increase in sensitivity, granting the ability to analyze smaller samples and detect lower concentrations of trace elements and minor isotopes.

This work performed under the auspices of the U.S. Department of Energy by Lawrence Livermore National Laobratory under Contract DE-AC52-07NA27344

# Development and benchmarking of a digitizer-based data acquisition system

Grayson Rich, *Nuclear Forensics Internship Program*
Kareem Kazkaz, *Physics Division, PLS Directorate*

Glenn T. Seaborg Institute

**We have developed and tested the components of a lightweight data acquisition (DAQ) system for use with flash analog-to-digital converters. These digitizers will be readily adaptable to new experiments, facilitate relative ease of data taking, and help to streamline analysis of the collected data. The C++-based software directly produces output files ready for processing using ROOT, CERN's data analysis toolkit ubiquitous in nuclear and high energy physics.**

## A simple experiment kept simple

A simple example of a digitizer-based DAQ system consists of a detector, a digitizer, and an acquisition computer running the DAQ software. This configuration could be used in a task such as gamma spectroscopy, and involves minimal setup time while using hardware that can later be utilized in myriad applications.

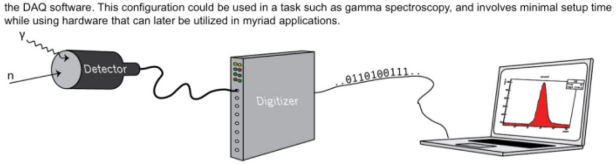


*Flow chart depicting the steps in the acquisition process and their approximate timescales or rates. The reported sampling and readout rates are characteristic of the SIS 3320 digitizer currently in use by the Advanced Detectors Group. The processing and disk writing performance are determined by the DAQ software and computer system.*


## Scalable and versatile

Taking advantage of the flexibility of digitizers and the generality of the software developed this summer, the complexity of a measurement can grow substantially while the components of the DAQ system remain unchanged. The number of digitizers in a system may increase, but a single module can handle, simultaneously, inputs from different types of detectors, e.g., $^3$He or $BF_3$ proportional counters, semiconductor detectors such as HPGe, or scintillators such as NaI(Tl).

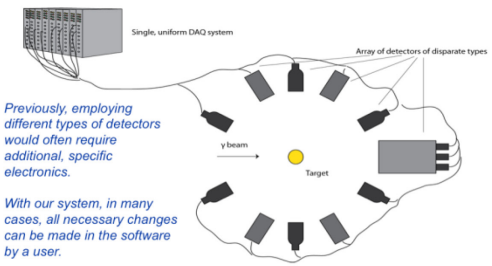


*Previously, employing different types of detectors would often require additional, specific electronics.*

*With our system, in many cases, all necessary changes can be made in the software by a user.*

Using the SIS 3320, the system can be utilized in a wide range of applications. With the software framework we have developed, support for additional digitizer models can be added with relative ease. Expanded capabilities such as sub-nanosecond timing resolution can be obtained with readily-available digitizers that feature sampling rates higher than 1 GHz.

## Analog vs. digital DAQs: an example

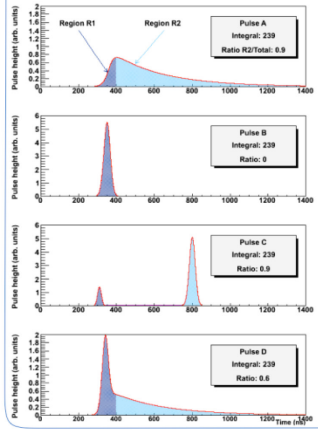


*Even with a priori knowledge of potential signal characteristics and heavy circuit modifications, a traditional, analog DAQ system will leave substantial uncertainties in analysis of the signals shown. Our new system, however, will allow development of reliable and accurate algorithms to distinguish between the pulse shapes and the underlying physical processes, enabling highly adaptive analysis and potential reduction in experimental uncertainties.*

- Users can set the system to save only key bits of information about the event, e.g., peak height, timestamp, and integral, **or** this information *plus the digitized pulse*.
- The ability to save waveforms affords great flexibility in later analysis, allowing for complete reanalysis of the raw data using different approaches long after the experiment has ended.
- Consider the four representative pulses shown at left, modeled after signals from a composite scintillator detector. A DAQ system designed to store only the integral of a signal would be unable to distinguish between any of the pulses. Additional electronics could expand its capabilities to include storing of the ratio of area R2 to the total area, allowing resolution between A and B, but this modified system is still unable to reliably discern between pulses A and C.
- The addition of pulse D and its R2/total ratio between that of pulses A and B introduces systematic uncertainty in data from the analog DAQ.

## Performance of system components

- The event and data throughput of both the readout and processing stages of the acquisition process was calculated by measuring the time spent in their respective stage. The digitizer had a resolution of 12 bits and a 200-MHz sampling rate, and was configured to store waveforms of 284 samples in length.
- We obtained readout rates of 5.0 x $10^4$ events per second, or 29 MBps, comparable to the 30 MBps maximum reported by the manufacturer of the digitizer. Our system was able to process these events at roughly 440 MBps (7.6 x $10^5$ events per second), when the step of writing data to disk is disabled. With this crucial component enabled, the throughput of the processing stage drops to 30 MBps (5.2 x $10^4$ events per second). Our system was therefore limited by the acquisition hardware, and not the software or computer.

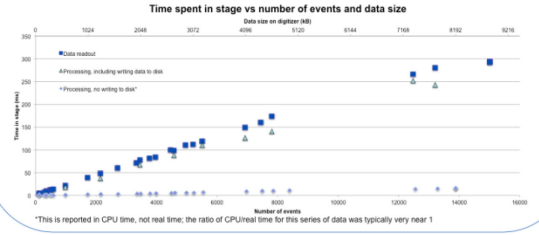


*This is reported in CPU time, not real time; the ratio of CPU/real time for this series of data was typically very near 1

## Reducing dead time through multithreading

*Multithreading allows for a higher frequency of data readout from the digitizer and a reduction in system "dead time", time during which the system is blind to new events and unable to record them.*

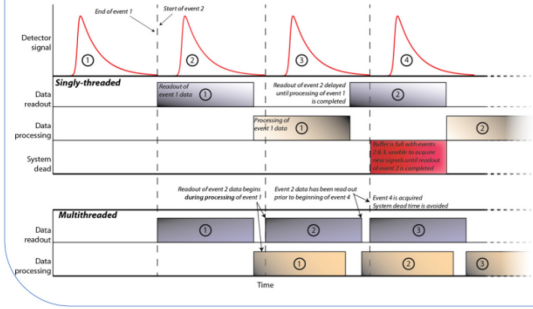


At left is a simplified timing diagram depicting a situation where dead time might occur and how it could be avoided by implementing a multithreaded approach, allowing the system to readout new data from the digitizer while concurrently processing previously obtained data. In this example, the digitizer is able to hold 2 events in its buffer and the singly-threaded system is 25% dead, having failed to acquire pulse 4. The multithreaded system is 0% dead, acquiring all events.

## Continued development

- Fully integrate components into a reliable, deployable package that can be controlled by an intuitive, console-based interface
- Test and debug the system to ensure its reliability for use by the Advanced Detectors Group on upcoming experiments
- Thoroughly document the system and its use so that it can more readily be adopted by new users
- Optimize singly-threaded implementation of system, perhaps using compression to increase processing throughput

## Longer-term goals

- Implement multithreading and investigate its effects on performance
- Develop a highly functional and easy-to-use graphical user interface
- Explore alternative ways to optimize performance using current hardware
- Update software to support newer, faster hardware

**This work performed under the auspices of the U.S. Department of Energy by Lawrence Livermore National Laboratory under Contract DE-AC52-07NA27344. LLNL-POST-492431**

# TEM Study of Neptunium Sorption to Goethite

Sandra Fernando, Nuclear Forensics Internship Program
Zurong Dai, Pihong Zhao, Mavrik Zavarin, and Annie Kersting, Chemical Sciences Division, PLS
Glenn T. Seaborg Institute

## Introduction

Neptunium migration in the environment is controlled by its (ad)sorption to minerals that can immobilize Np in the solid phase or mobilize it via colloid-facilitated transport[1]. A detailed understanding of these processes, at the molecular-scale, is essential for developing remediation strategies and reliable predictive transport models. The adsorption of long-lived actinides such as plutonium and Np-237 ($t_{1/2}$=2.14x$10^6$ years) is of particular interest because of their persistence in the environment. Pu and Np have both been shown to (ad)sorb strongly to goethite (a-FeOOH), a common iron oxide mineral found in the environment. Pu(V) is the most common oxidation state of Pu(V) in the aqueous state. However, it is often observed to reduce to Pu(IV) in the presence of mineral surfaces. Np(V) is the most common oxidation state[3] in the environment in both aqueous and sorbed states. However, it has been shown to reduce to Np(IV) under anoxic conditions.

Transmission electron microscopy (TEM) was previously used to image and characterize Pu complexes on goethite. The sorption behavior of Pu(V) on goethite is unusual. Pu(V)-goethite interaction will result in Pu(V) reduction and epitaxial growth of nano-scale $Pu_4O_7$ crystals on the goethite surface[2]. In the present study, we examine whether similar behavior may be observed for Np(V). We use batch sorption combined with TEM characterization to examine sorbed Np(V) complexes on goethite. The work builds upon earlier batch Np(V)-goethite sorption experiments performed by Mathew Snow (2010 summer student) at low Np(V) concentrations. X-ray absorption spectroscopy indicates neptunium sorbs onto goethite as a isolated neptunyl ($NpO_2^{2+}$) groups and possibly as disordered Np (hydr)oxide precipitates[4]. Np(V) sorption to goethite is difficult to characterize by TEM due to neptunium's relatively weak sorption (compared to Pu). As a result, a significant part of this project is dedicated towards optimizing sample preparation such that the sorbed Np concentrations are above the TEM's detection limits.

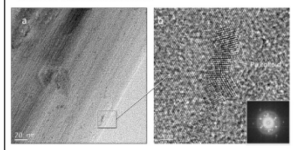

TEM bright field (a) and HRTEM (b) of 1,900 ppm Pu(IV)/goethite indicating formation of $Pu_4O_7$ nanocolloids on the goethite surface.

## Objectives

- Study Np-goethite interactions at high concentrations ($10^{-5}$ to $10^{-8}$ M)
- Evaluate effect of common reductant (sodium dithionite) on sorption behavior.
- Develop TEM sample preparation method(s) enabling observation of weakly sorbing Np(V)
- Characterize Np-goethite interaction using TEM

## Results

### Sample preparation

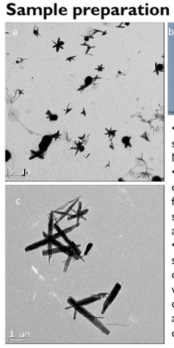

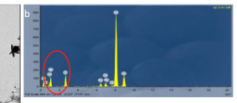

- Salt removal test 1 contained a lot of salt (a), which X-ray EDS indicated was NaCl (b).
- Salt removal test 2 provided much cleaner goethite crystals; no salt was found (c). This sample prep solution/method was used for the adsorption studies.
- During sample preparation, there were several contamination incidents: Cu chloride salts, and Ti, Si, and Al oxides were found on grid. Source of contamination is possibly from pipet tips and/or reactions occurring with the copper grids used.

### Adsorption experiment

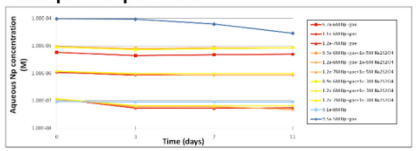


### Rate Dependence of Sorption

- Equilibrium reached within 3 days for lower concentration samples.
- Np spiked blank sample showed ~1% activity loss due to sorption on container walls.
- Highest Np spiked sample observed decrease in aqueous concentration at 11 days while all other samples reached equilibrium.

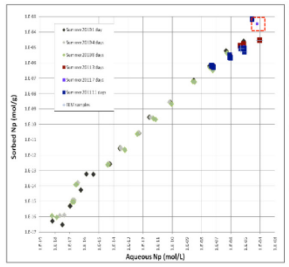


### Sorbed Np vs. aqueous Np

- Sorbed Np concentrations are lower than those observed last summer.
- Solutions containing dithionite observed lower sorption.
- Sorption decreased with time for the 1st adsorption experiment while the 2nd adsorption experiment observed an increase.
- Red box indicates region where Np sorption was observed on Summer 2011 samples (i.e. TEM sample images displayed to the right).

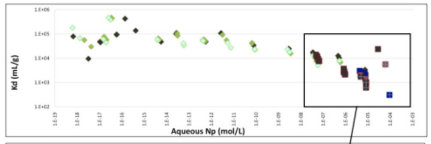


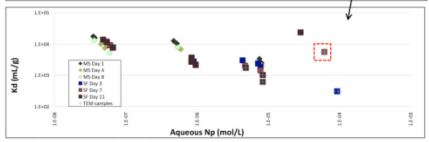


### Kd as a function of aqueous Np

- Kd decreases exponentially at higher Np concentrations, except for highest Np-spiked sample.
- Kds for dithionite containing solutions are smaller than Kds for solutions without dithionite.

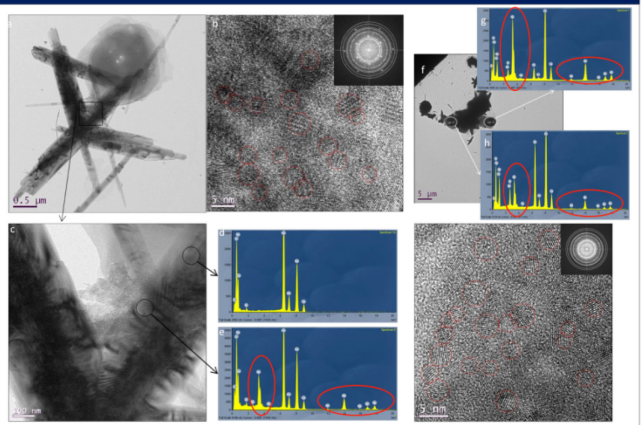

- Goethite crystals had typical star-shaped morphology (a) and composition (d).
- Np was detected only on the highest Np-spiked sample (2nd adsorption experiment; not centrifuged) after equilibrating for 3 (not shown) and 7 days (a-e); including Np that could precipitate directly from solution onto goethite, the estimated load was ~2.3e5ppm.
- Np colloids attached to goethite (c) and were detected to be associated with goethite by X-ray EDS (e).
- Crystalline Np colloids can be identified to distribute on goethite in HRTEM image (b); the ring pattern shown in FFT (inset of b) is from crystalline Np colloids adsorbed and/or attached on goethite;
- Initial analysis of FFT indicates crystal structure is cubic $NpO_2$ .
- Significant amount of Np found in supernatant (f-h) and on C-film (i); also has $NpO_2$ crystal structure.

## Methods

**1) Np-237 Purification**
- 2 mL 100-200 mesh AG BioRad column, concentrated HCl load solution
- Pa-233 daugher eluted using 9M HCl + 0.05 M HF
- Purified Np-237 eluted using 6M HCl +0.05 M HF

**2) Np(V) spike preparation**
- Reconstituted in $HNO_3$ to fix the Np oxidation state at (V) and (VI)
- $H_2O_2$ added to reduce Np(VI) (if present) to Np(V).
- Spike solution centrifuged and filtered in swinging bucket rotor at 4000 RPM for 1.5 hours to remove Np(IV).

*For 2nd adsorption experiment:*
- New Np(V) spike was dried and redissolved in 18 MQ H2O to minimize acid content
- UV-Vis used to verify Np-237 oxidation state when spike concentration was ≥ $10^{-3}$ M.
- Np(V) spike solution titrated to ~pH 3 with NaOH

**2) Np(V) Sorption**
**Ist adsorption experiment**
- Goethite suspended in 5mM NaCl + 0.7mM NaHCO3 solution (pH 8.0±0.8)
- $10^{-6}$ - $10^{-8}$ M Np(V)
- 0 to $10^{-3}$ M sodium dithionite
- Solutions constantly mixed using rotary mixer
- 3, 7, and 11 day sampling
- Samples centrifuged at 3700 RPM for 2hrs
- Np-237 in the supernatants analyzed by LSC

**2nd adsorption experiment**
- Goethite suspension washed 3xs in 18 MQ H2O and resuspended in MQ H2O adjusted to pH 8 with NaOH.
- $10^{-5}$ M Np(V)
- No sodium dithionite addition.

**TEM preparation and methods**
**Sample prep testing**
- Goethite samples originally in pH 8 5mM NaCl + 0.7 mM NaHCO3 buffer. To examine salt effect on TEM sample preparation:
  1. Goethite aliquot was diluted 10x with buffer and sonicated.
  2. Goethite suspension centrifuged at 10K RPM for 20 min, decanted, replaced with pH 8 MQ H2O, sonicated, and diluted 10x in pH 8 MQ H2O.
- 2 µL of solution were each deposited on carbon-coated, copper grids with aluminum foil beneath (TEM) or carbon tape (SEM mounts).

**1st adsorption experiment**
- After 11 days equilibration, highest Np concentration samples were prepared for TEM using method 2.
- 2 µL of diluted solution were deposited on formvar, carbon-coated, copper grids with either weighing paper or aluminum foil beneath.

**2nd adsorption experiment**
- After 3 and 7 days equilibration, 2 µL of the suspension (not centrifuged) was placed on formvar
- A second sample was prepared by method 2 (but not diluted).

## Conclusions

- **Kd was found to decrease significantly from $10^{-8}$ to $10^{-5}$ M, and compared well with lower concentration data from Matthew Snow.**
- **Must reconsider how much Np is sorbed onto goethite versus Np precipitated in solution, especially at ≥$10^{-5}$ M Np.**
- **Sorption/attachment of $NpO_2$ onto goethite was found.**
- **Effects from sodium dithionite were not significant on this time scale.**
- **Np-goethite sorption is much weaker than Pu-goethite sorption; could depend on kinetics of Np crystal growth.**
- **Artifacts possibly present: Np could have evaporated out of solution onto goethite crystals.**
- **Future work includes:**
  - **Examine Np sorption to goethite over longer time intervals using TEM and LSC, and characterize crystal structures of Np colloids on goethite.**
  - **Understand Np(V) reduction and/or Np(IV) precipitation under these conditions.**

## References

1- Kersting AB., D. W. Efurd, D. L. Finnegan, D. J. Rokop, D. K. Smith, J. L. and Thompson, (1999). *Nature 397, 56-59*
2 – B.A. Powell, Z. Dai, M. Zavarin, P. Zhao, and A.B. Kersting, (2011). Environmental Science and Technology 45, 2698-2703.
3 - Dozol M, Hagemann R: *Pure Appl Chem 1993 , 65:1081-1102*
4- J.M. Combes, C.J. Chrisholm-Brause, G.E. Brown, G.A. Parks, S.D. Conradson, P.G. Eller, I.R. Triay, D.E. Hobart, and A. Meijer, (1992). Environmental Science and Technology 26, 376-382

This work performed under the auspices of the U.S. Department of Energy by Lawrence Livermore National Laboratory under Contract DE-AC52-07NA27344.

Release #:

# $^{35}S$: A New Tracer for Monitoring of Groundwater Recharge in Alpine Basins

Glenn T. Seaborg Institute

Stephanie H. Diaz, Nuclear Forensics Internship Program

Bradley K. Esser, Richard K. Bibby, Chemical Sciences Division, PLS

## Introduction

- Numerous lines of evidence suggest that the hydrology of the Southwestern U.S. will change due to anthropogenic climate change. For example, snow packs in the Northern Sierra Nevada are declining and more "rain-on-snow" events are occurring (e.g., Mote *et al.* 2005; Knowles *et al.* 2006), which may reduce groundwater recharge and lead to reductions in baseflow during the late summer and early fall (Earman *et al.* 2006).
- Groundwater contributes significantly to water flux in rivers and streams (e.g., Genereux and Hooper, 1998); therefore reduced groundwater recharge affects both groundwater and surface water resources.
- Predictions of late summer stream flow may improve by identifying the:
  1) Fraction of annual snowpack retained in the groundwater system for >1 yr
  2) Fraction of snowpack rapidly exported from the basin as baseflow.

### *Project Goals*

- Evaluate the potential of $^{35}S$ as a tracer
  - Determine fraction of stream flow derived from previous spring's snowmelt
  - Assess storage capacity and retention time
- This work is being conducted as part of a larger geochemical study to develop and refine techniques for groundwater monitoring

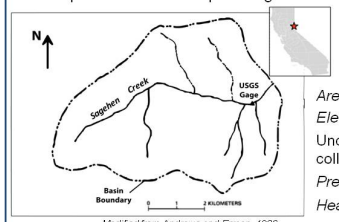


*Modified from Andrews and Erman, 1986*

### *Field Site*

**Sagehen Creek Basin**

*Area*: ~27 km$^2$

*Elevation*: 1900m-2600m

Unconsolidated: glacial till, alluvium, colluvium

*Precipitation*: 88cm/yr (80% snow)

*Headwater Tributary*: Sagehen Creek

## $^{35}S$ Geochemistry

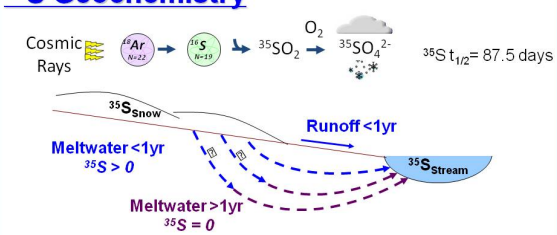


$$\text{Fraction Recent Winter Snowmelt (RWS)} = \frac{^{35}S_{Stream}\ (\text{mBq/mg } SO_4^{2-})}{^{35}S_{Snow}\ (\text{mBq/mg } SO_4^{2-})}$$

## Field Sampling

From 2009 to 2011, samples were collected from Sagehen Creek, a perennial spring, and snowpack within Sagehen Creek Basin.


## Lab Analysis

Samples were processed using modified techniques from Michel et al. (2000):

1) $SO_4^{2-}$ extracted by suspending Amberlite anion exchange resin in the sample
2) $SO_4^{2-}$ eluted from the resin with a NaCl solution
3) $BaCl_2$ added to precipitate $BaSO_4$
4) $BaSO_4$ suspended in instagel for liquid scintillation counting

Detection limit between 0.1 mBq/L and 2.9 mBq/L depending on counting conditions

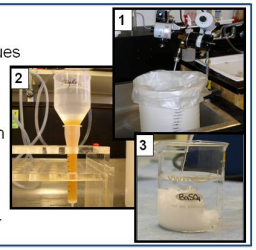


## Results

- Snow $^{35}S$ activity ranged from 5.7 mBq/L to 12.4 mBq/L, and Sagehen Creek activities ranged from <0.3 mBq/L to 7.4 mBq/L at collection time implying a fraction of recent winter's snow (RWS) <1% during peak flow conditions to >100% during baseflow conditions (Table 1).
- Fractions of RWS >100% may be due to variations in $^{35}S$ activity of the snowpack end member or precipitation events during baseflow.
- Increasing discharge during the spring snowmelt period did not coincide with an increase in $^{35}S$ activity for the sampling period (Figure 1), suggesting storage and piston flow movement through the basin.
- Similar trends of increasing $^{35}S$ activity after peak discharge were observed when accounting for $SO_4^{2-}$ concentration

**Table 1.** Average $^{35}S$ activities during baseflow and peak flow for Sagehen Creek and the perrenial spring ± standard deviations. All activities are decay-corrected to date of sample collection.

| Sample Type | Sample Period | $^{35}S$ (mBq/L) | Fraction RWS |
|---|---|---|---|
| Sagehen Creek | Baseflow | 0.9±0.6 | 86% |
| | Peak Flow | 0.5 ±0.02 | 10% |
| Perrenial Spring | Baseflow | 0.8±0.1 | 46% |
| | Peak Flow | <0.7 | 17% |

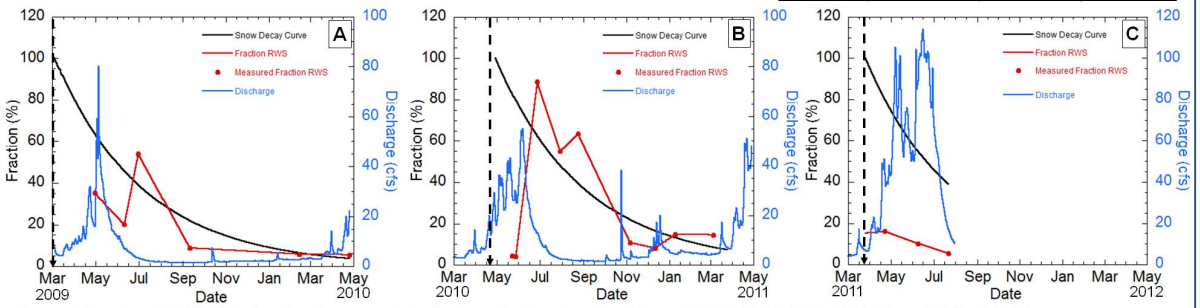


**Figure 1.** Fraction of RWS plotted against the mean daily discharge for Sagehen Creek from 2009-2010 (A), 2010-2011 (B), and 2011-2012 (C). Dashed line represents initiation of snowmelt for given year.

## Conclusions

- Sagehen Creek Basin has the capacity to store meltwater for more than one year
- Evaluation of $^{35}S$ method:
  - Tracer was useful in assessing alpine catchment hydrology on short time scales
  - May allow researchers to better determine how climate warming could affect groundwater recharge and input to stream flow

### *Future Work*

- $^{35}SO_4^{2-}$ soil retention study to provide evidence that $^{35}SO_4^{2-}$ is not being retained along the flow path
- Survey other Sierra basins to determine the fraction of base flow stored in the groundwater for more than one season
- Integrate data with hydrologic models to demonstrate how stream flow will respond to climate warming

## References

Earman, S., A.R. Campbell, B.D. Newman, and F.M. Phillips, 2006. Isotope exchange between snow and atmospheric water vapor: estimation of the snowmelt component of groundwater recharge in the southwestern United States. *J Geophys Res*, 111: D09302

Genereux, D.P. and R.P. Hooper, 1998. Oxygen and hydrogen isotopes in rainfall-runoff studies, in Kendall, C., and J.J. McDonnell, eds., *Isotope Tracers in Catchment Hydrology*: Amsterdam, Elsevier, pp.319-346.

Knowles, N., M.D. Dettinger, and D.R. Cayan, 2006. Trends in snowfall versus rainfall in the western United States. *J Climate*,19(18):4545-4559.

Michel, R.L., D. Campbell, D. Clow, and J.T. Turk, 2000. Timescales for migration of atmospherically derived sulphate through an alpine/ subalpine watershed, Loch Vale, Colorado. *Water Resour Res*,36:27-36.

Mote, P.W., A.F. Hamlet, M.P. Clark, and D.P. Lettenmaier, 2005. Declining mountain snowpack in western North America. *B Am Meteorol Soc*, 86(1): 39-49

This work performed under the auspices of the U.S. Department of Energy by Lawrence Livermore National Laboratory under Contract DE-AC52-07NA27344